

REPORT



Single cell-produced and *in vitro*-assembled anti-FcRH5/CD3 T-cell dependent bispecific antibodies have similar *in vitro* and *in vivo* properties

Ayse Meric Ovacik, Ji Li, Marie Lemper, Dimitry Danilenko, Nicola Stagg , Mary Mathieu, Diego Ellerman , Vinita Gupta, Navdeep Kalia, Trung Nguy , Vicki Plaks, Clarissa David Johnson, Weiru Wang , Jochen Brumm , Bernard Fine, Teemu Junttila, Kedan Lin , Paul J. Carter , Saileta Prabhu, Christoph Spiess , and Amrita V. Kamath

Genentech Research and Early Development, Genentech, Inc., South San Francisco, CA, USA

ABSTRACT

Bispecific antibody production using single host cells has been a new advancement in the antibody engineering field. We previously showed comparable *in vitro* biological activity and *in vivo* mouse pharmacokinetics (PK) for two novel single cell variants (v10 and v11) and one traditional dual cell *in vitro*-assembled anti-human epidermal growth factor receptor 2/CD3 T-cell dependent bispecific (TDB) antibodies. Here, we extended our previous work to assess single cell-produced bispecific variants of a novel TDB against FcRH5, a B-cell lineage marker expressed on multiple myeloma (MM) tumor cells. An *in vitro*-assembled anti-FcRH5/CD3 TDB antibody was previously developed as a potential treatment option for MM. Two bispecific antibody variants (designs v10 and v11) for manufacturing anti-FcRH5/CD3 TDB in single cells were compared to *in vitro*-assembled TDB in a dual-cell process to understand whether differences in antibody design and production led to any major differences in their *in vitro* biological activity, *in vivo* mouse PK, and PK/pharmacodynamics (PD) or immunogenicity in cynomolgus monkeys (cynos). The binding, *in vitro* potencies, *in vitro* pharmacological activities and *in vivo* PK in mice and cynos of these single cell TDBs were comparable to those of the *in vitro*-assembled TDB. In addition, the single cell and *in vitro*-assembled TDBs exhibited robust PD activity and comparable immunogenicity in cynos. Overall, these studies demonstrate that single cell-produced and *in vitro*-assembled anti-FcRH5/CD3 T-cell dependent bispecific antibodies have similar *in vitro* and *in vivo* properties, and support further development of single-cell production method for anti-FcRH5/CD3 TDBs and other single-cell bispecifics.

ARTICLE HISTORY

Received 14 September 2018
Revised 9 November 2018
Accepted 20 November 2018

KEYWORDS

T cell-dependent bispecific;
pharmacokinetics and
pharmacodynamics;
antibody drug development;
multiple myeloma

Introduction

Multiple myeloma (MM) is characterized by abnormal growth of plasma cells (PCs) in the bone marrow (BM) and the overproduction of immunoglobulin by these abnormal PCs, leading to hypercalcemia, anemia, renal impairment or bone pain.¹ While the life expectancy of MM patients is increasing due to the availability of novel agents,^{2,3} the disease remains incurable in most patients owing to repeated relapses.⁴ Modalities that recruit T cells, including chimeric antigen receptor therapies, to kill tumors have shown promise in patients with B cell malignancies.^{5–7} There is also growing interest on developing bispecifics and T-cell recruiting therapeutics for solid tumors.^{8–10}

Previously, we described the design, mechanism of action (MOA) and pharmacokinetics (PK)/pharmacodynamics (PD) of an *in vitro*-assembled anti-FcRH5/CD3 TDB.¹¹ The anti-CD3 arm of this T-cell dependent bispecific (TDB) engages T cells and the anti-FcRH5 arm engages FcRH5-expressing cells such as B cells, PCs and MM cells to form an immunological synapse.¹¹ When the synapse is formed, T cells are activated, resulting in FcRH5-dependent cell killing either through cytokine release

caused by T-cell activation or through direct killing by granzymes and perforin-induced cell lysis.¹² The anti-FcRH5/CD3 TDB exhibited cytotoxic activity against normal human PCs and patient-derived primary MM cells.¹¹ Additionally, the anti-FcRH5/CD3 TDB showed robust PD activity, including complete depletion of B cells and PCs in cynomolgus (cyno) BM.

In vitro-assembled anti-FcRH5/CD3 TDB is produced by a two-cell process, where the two component antibodies (anti-FcRH5 ‘knob’ and anti-CD3 ‘hole’) are first expressed in separate host cells. These half-antibodies containing knobs-into-holes (KIH) mutations are then purified, and the anti-FcRH5/CD3 TDB is subsequently assembled *in vitro*.^{13–15} This design includes mutations in the C_H3 domain of the Fc region for preferential heavy chain heterodimerization to ensure efficient bispecific antibody production (Figure 1). *In vitro*-assembly is well established and has been used to produce a large number of bispecific IgGs at Genentech.^{15–17} In recent years, several different groups, including ours, have developed novel methods to efficiently produce bispecific IgGs in single host cells.^{18–23} Single-cell production of bispecific IgGs offers simpler, faster, and more cost efficient manufacturing. We previously reported two novel

CONTACT Ayse Meric Ovacik  ovacika@gene.com; Amrita V. Kamath  amritak@gene.com  Genentech, Inc., 1 DNA Way, South San Francisco, CA 94080, USA

 Supplemental data for this article can be accessed on the [publisher's website](#).

© 2018 The Author(s). Published by Taylor & Francis.

This is an Open Access article distributed under the terms of the Creative Commons Attribution-NonCommercial-NoDerivatives License (<http://creativecommons.org/licenses/by-nc-nd/4.0/>), which permits non-commercial re-use, distribution, and reproduction in any medium, provided the original work is properly cited, and is not altered, transformed, or built upon in any way.

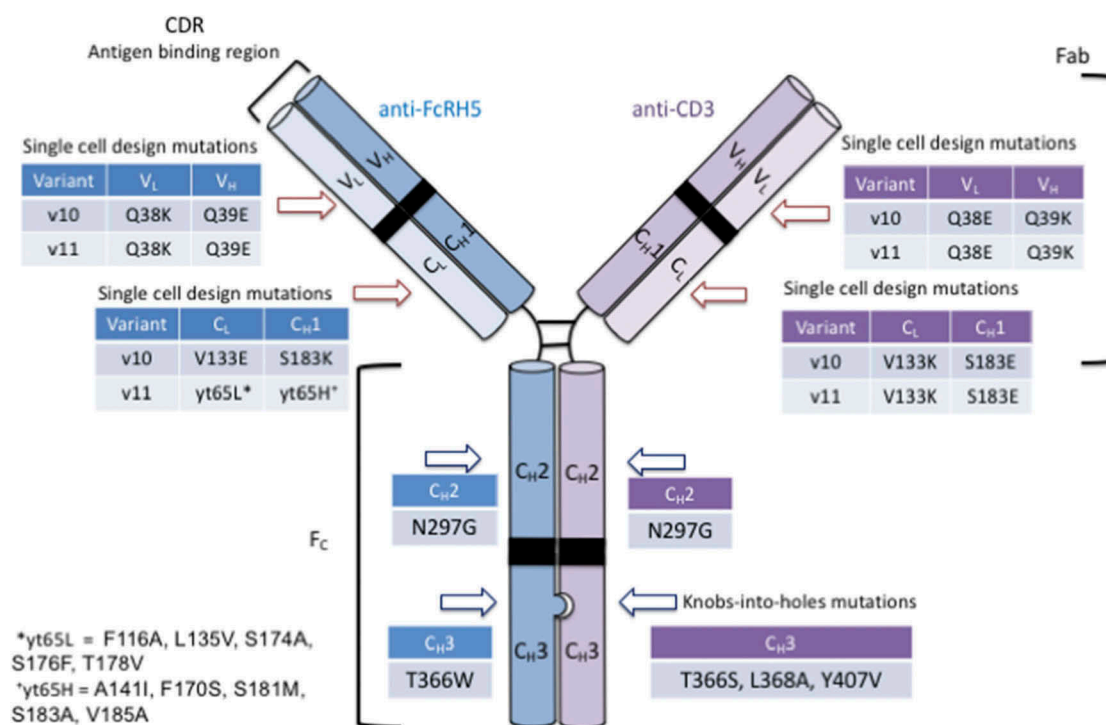


Figure 1. Schematic representation of bispecific IgG. Different arms of the bispecific antibody are shown in different colors (Blue and light blue arm denote heavy chain and light chain of one arm, respectively. Purple and light purple arm denote heavy and light chains of the other arm, respectively and the domains are indicated. The arrows point to domain interfaces of the mutations. The details of the knobs-into-holes mutations and single cell bispecific design mutations were described previously.^{14,16}

designs for single cell bispecific antibodies (v10 and v11) that included modifications in the antigen-binding fragment (Fab) arms to promote selective pairing of cognate heavy and light chains in addition to the KIH mutations in the antibody Fc.¹⁸ Specifically, the charge-pair modifications of the single cell design v10 are located at the V_H-V_L interface, outside of the complementarity-determining regions (CDRs) and at the C_{H1}-C_L interface (Figure 1). These charge-pairs do not perturb the structure of the molecule and have a minimal solvent accessible surface area.¹⁸ Design v11 differs from v10 by utilizing a remodeled C_{H1}-C_L interface instead of a charge pair in one of the C_{H1}-C_L interfaces. We produced single cell variants (v10 and v11) of another TDB, namely anti-human epidermal growth factor receptor 2 (HER2)/CD3 TDB, using a different anti-CD3 antibody than the anti-FcRH5/CD3 TDB.¹⁸ The designs did not affect binding of the HER2 antigen, and they had comparable *in vitro* biological activities and similar PK in mice compared to *in vitro*-assembled anti-HER2/CD3 TDB.

Here, we extended our previous work to assess single cell produced bispecific variants of a novel TDB against FcRH5. In addition to the *in vitro* and *in vivo* characterization conducted previously for the anti-HER2/CD3 TDBs,¹⁸ we included assessment of cyno PK/PD and immunogenicity. The single cell anti-FcRH5/CD3 TDBs have the same CDRs as the *in vitro*-assembled anti-FcRH5/CD3 TDB. Moreover, the single cell anti-FcRH5/CD3 TDBs have a heavy chain mutation (N297G) to prevent N-linked glycosylation like the *in vitro*-assembled anti-FcRH5/CD3 TDB. We found that the N297G mutation decreased FcγR binding of therapeutics antibodies, and resulted in virtually no antibody-dependent cell-mediated cytotoxicity

(ADCC) activity.²⁴ This mutation ensures that the cytotoxic action of the TDB is only due to T cell engagement, and Fc receptor-mediated ADCC does not contribute to TDB activity. Overall structural features of the single cell-produced TDBs are similar to the *in vitro*-assembled TDB. We produced two single cell variants (v10 and v11) of anti-FcRH5/CD3 TDB according to our previously described designs.¹⁸ *In vitro* and *in vivo* properties of the *in vitro*-assembled anti-FcRH5/CD3 TDB were previously characterized.¹¹ We evaluated *in vitro* and *in vivo* properties of the two single cell TDBs along with the *in vitro*-assembled TDB to determine whether differences in bispecific antibody design and production lead to any major differences in these endpoints.

Results

Single cell-produced and *in vitro*-assembled anti-FcRH5/CD3 tdb have comparable binding properties

The binding affinities of the single cell-produced TDBs (termed single cell TDBs) to human and cyno FcRH5 and CD3ε were comparable to the corresponding binding affinities of *in vitro*-assembled anti-FcRH5/CD3 TDB as measured by surface plasmon resonance (SPR) or radioligand cell-binding assay (Table 1). In addition, no differences in affinities for FcRH5 or CD3ε were observed between the two single cell TDBs, v10 and v11.

The affinities of the anti-CD3 arm in all 3 variants were generally lower for the human CD3ε compared to the cyno CD3ε, whereas the affinities of the FcRH5 arm for all 3

Table 1. Single cell- and *in vitro*-assembled anti-FcRH5/CD3 TDBs had comparable antigen binding affinities for human and cyno FcRH5 and CD3 ϵ . Radio ligand cell-binding assays were used to determine the K_D of the 3 anti-FcRH5/CD3 TDBs to human and cyno FcRH5. Surface plasmon resonance was used to determine K_D of the three anti-FcRH5/CD3 TDBs to human and cyno CD3 ϵ . Measurements were taken at 25°C and pH 7.4 for both methods. The affinities reported here were monovalent affinities of each arm.

Anti-FcRH5/CD3 TDB	FcRH5, K_D (nM)			CD3 ϵ , K_D (nM)		
	Human	Cyno	Human/ Cyno*	Human	Cyno	Human/ Cyno*
<i>In vitro</i> -assembled	3.1	8.2	0.4	1.8	0.7	2.5
Single cell v10	2.6	7.1	0.4	2.2	0.4	5.3
Single cell v11	3.3	7.9	0.4	2.5	0.6	4.5

*, Ratio of human to cyno binding, dimensionless

variants were lower for cyno FcRH5 compared to human FcRH5.

Single cell and *in vitro*-assembled anti-FcRH5/CD3 TDB showed robust *in vitro* pharmacological activity

We evaluated the *in vitro* pharmacological activities of two single cell TDBs along with the *in vitro*-assembled TDB in two different assays: 1) cytotoxicity of FcRH5-expressing PCs, and 2) cytotoxicity and T-cell activation of the FcRH5-expressing

MM cell line MOLP-2. The concentration-cell killing percentage and $E_{MAX} - EC_{50}$ model fits are shown in Figure 2. The summary of estimated parameters is provided in Table 2 (see Fig. S2 for each estimated $E_{max} - EC_{50}$ value).

The capacity of the anti-FcRH5/CD3 TDBs to kill PCs was analyzed by targeting BM mononuclear cells (BMMCs) isolated from BM aspirates of one cyno (Figure 2(a)) and two healthy human donors (Figure 2(b), representative profile). The expression patterns of FcRH5 were previously shown to be similar in humans and cynos.¹¹ The single cell and *in vitro*-assembled TDBs had robust and comparable PC cytotoxicity profiles for cyno and human cells. In addition, the maximum cell killing values of all the TDBs were slightly higher, although not substantially, for human PC (~80%) compared to cyno PC (~60%).

The capacity of the anti-FcRH5/CD3 TDBs to kill MOLP-2 cells (Figure 2(c)) and induce T-cell activation (Figure 2(d)) were analyzed by cytotoxic activity of MOLP-2 cells co-cultured with isolated human CD8⁺ T cells from three human donors. The single cell and *in vitro*-assembled TDBs exhibited robust and comparable MOLP-2 cell killing profiles, although high variability was observed across donors (Fig. S1B and E). In addition, single cell TDBs exhibited marginally

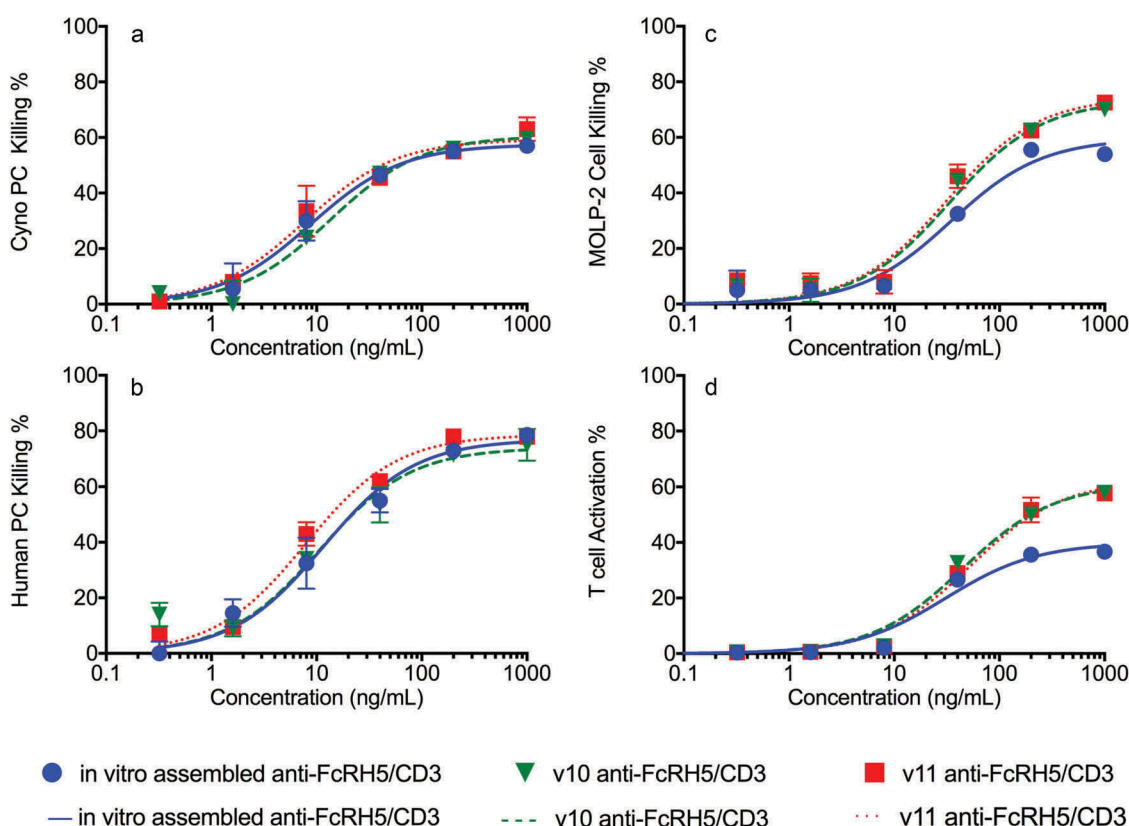


Figure 2. Single cell and *in vitro*-assembled TDBs have robust *in vitro* activities. Concentration-response (*in vitro* activity) data were determined in independent duplicates of sample size, n . Mean and standard deviation of the duplicate measurements are presented as symbols (blue circles denote *in vitro*-assembled TDB, green reverse triangles denote single cell TDB v10, red squares denote single cell TDB v11). Sigmoidal E_{max} model fits were shown as blue solid (*in vitro*-assembled TDB), green dashed (single cell TDB v10), and red dotted line (single cell TDB v11). Estimated E_{max} and EC_{50} values are summarized in Table 2 and are also provided in Fig. S2 for concentration-response (*in vitro* activity) data. (a) Cytotoxicity data for single cell and *in vitro*-assembled TDBs mediated killing of cyno PCs. The data were obtained from one cyno BM aspirate. (b) Cytotoxicity data for single cell and *in vitro*-assembled TDBs mediated killing of human PCs. The data were obtained from two donors ($n = 2$). One representative profile is shown. (c) Cytotoxicity data for single cell and *in vitro*-assembled TDBs mediated killing of MOLP-2 cells co-cultured with isolated human CD8⁺ T cells. The data were obtained from 3 donors ($n = 3$). One representative profile is shown. (d) Anti-FcRH5/CD3 TDB dependent T cell (CD8⁺) activation when co-cultured with the MOLP-2 cell line for single cell and *in vitro*-assembled TDBs. The data were obtained from the same 3 donors as in MOLP-2 cell cytotoxic activity ($n = 3$). One representative profile is shown.

Table 2. Single cell and *in vitro*-assembled anti-FcRH5/CD3 TDBs had similar *in vitro* cytotoxic activities. Data show estimated E_{max} and EC_{50} values of cytotoxic activity and T-cell activation for single cell and *in vitro*-assembled TDBs. CD8⁺ cells were used as effectors in a 3:1 effector:target ratio in MOLP-2 cell line cytotoxicity assay. Data are presented as mean and standard deviation where applicable. Individual E_{max} and EC_{50} values were provided in Fig. S1.

Anti-FcRH5/ CD3 TDB	Hill equation parameter	<i>In vitro</i> activity			
		Cyno PC cytotoxicity n = 1	Human PC cytotoxicity n = 2	MOLP-2 cytotoxicity n = 3	T-cell activation n = 3
<i>In vitro</i> -assembled	E_{MAX}	57.5	79.3 ± 1.6	75.5 ± 15.3	32.9 ± 6
	EC_{50} (ng/mL)	8.8	16.5 ± 6.9	21.7 ± 12.3	27.2 ± 6.3
Single cell v10	E_{MAX}	60.6	78.2 ± 5.9	86.4 ± 11.8	47.7 ± 11.7
	EC_{50} (ng/mL)	13.5	19.7 ± 12.9	21.1 ± 11.2	38.2 ± 6.65
Single cell v11	E_{MAX}	59.3	78.3 ± 0.7	86.9 ± 11.1	47.9 ± 12.8
	EC_{50} (ng/mL)	7.7	15.6 ± 10.9	18.8 ± 11.3	44.0 ± 10.1

higher (~10–20%) maximal T-cell activation (E_{max}) (Fig. S1C), and slightly lower, albeit not meaningful, (~1.5 fold) potency (EC_{50}) (Fig. S1F), when compared to *in vitro*-assembled TDB. No difference was observed between the single cell TDBs in T-cell activation.

Single cell and *in vitro*-assembled anti-FcRH5/CD3 TDB had similar PK properties in SCID.bg mice

The anti-FcRH5/CD3 TDBs do not cross-react with mouse FcRH5 or CD3 ϵ . Hence, the mouse PK profiles of the anti-FcRH5/CD3 TDBs provided an opportunity to compare the PK of the two single cell TDBs to *in vitro*-assembled TDB in the absence of target binding. Serum concentration-time profiles of the three anti-FcRH5/CD3 TDBs were assessed along with two control antibodies: anti-gD (a non-binding control IgG, targeting the glycoprotein D epitope of herpes simplex virus)¹³ and anti-gD/CD3 TDB (IgG1 framework, KIH bispecific antibody with the same anti-CD3 arm as the *in vitro*-assembled anti-FcRH5/CD3 TDB). The PK data of each group were characterized by non-compartmental analysis (NCA) (Table 3) and in a two-compartment (2-C) model (Table S1). The PK data of all groups exhibited biphasic profiles (See Fig. S2 for the two-compartment model fits).

The systemic exposures of the single cell TDBs were generally comparable to the exposure of the *in vitro*-assembled TDB (Table 2 and Figure 3). Moreover, simulations of compartmental model parameters for each group (single cell v10, v11 and *in vitro*-assembled TDB) at 5 mg/kg dosing showed that exposures of the 3 TDBs overlapped (Fig. S3).

The anti-gD administered group had higher exposure compared to all anti-FcRH5/CD3 TDB administered groups, as well as the anti-gD/CD3 administered group. Given the lower exposure of the CD3-containing TDBs compared to the bivalent anti-gD control, we asked if there were characteristics of the CD3 arm that could have contributed non-specifically to the observed lower exposure. We estimated the antibody variable region (Fv) charge and hydrophobicity of anti-CD3 using iCAT (*in silico* clearance assessment tool,²⁵ see Material and Methods). The calculated Fv charge was +7.6, which is outside the range for acceptable *in vivo* clearance (Fv charge ≤ 0 or ≥ +6.2). In addition, the structure of the anti-CD3 arm Fab region (Figure 4) showed a positively charged region that was surface exposed.

Single cell and *in vitro*-assembled TDB had similar PK properties in cynos

The anti-FcRH5/CD3 TDBs cross-reacted with cyno FcRH5 and CD3 ϵ . Hence, the cyno PK profiles provided an opportunity to compare the PK of the single cell TDBs to the *in vitro*-assembled TDB in the presence of both targets. Serum concentration-time profiles of the anti-FcRH5/CD3 TDBs following a single intravenous (IV) bolus dose of 2 mg/kg in cyno are shown in Figure 5. All the animals that were given TDBs tested positive for anti-drug antibodies (ADA) (Fig. S4), whereas the vehicle-administered control animals and pre-dose samples from all animals were negative. ADA was observed as early as day 7 and was apparent in all the cynos administered TDBs by day 13. Therefore, the observed C_{max} and AUC_{0-4} were used to compare the different variants.

Table 3. Similar PK parameters of single cell- and *in vitro*-assembled TDBs in SCID mice. PK parameters for control antibodies anti-gD and anti-gD/CD3 are shown. The PK data were characterized with NCA. Sparse sampling was used to generate PK profiles and actual dose concentrations were used in data analysis (see Material and Methods). Standard error values are provided where applicable. C_{max} = Maximum observed serum concentration, AUC_{0-last} = Area under the serum-concentration time curve from time 0 to last measured time points, day 21. Parameters from compartmental analysis and associated model fits are provided in Table S1 and Fig. S2, respectively.

PK parameter	Control groups		Anti-FcRH5/CD3 TDB		
	Anti-gD	Anti-gD/CD3	<i>In vitro</i> -assembled	Single cell v10	Single cell v11
Actual dose (mg/kg)	4.4	5.7	5.05	4.65	6.5
C_{max} (μ g/mL)	87.3 ± 6.3	82.9 ± 3.6	74.5 ± 2.7	65.9 ± 0.5	85.9 ± 4.0
$C_{max}/Dose$ (μ g/mL)/(mg/kg)	19.8	14.5	14.7	14.1	13.1
AUC_{0-last} (day· μ g/mL)	633 ± 34	409 ± 12	318 ± 7	273 ± 4.5	358 ± 19
$AUC_{0-last}/Dose$ (day· μ g/mL)/(mg/kg)	144	72.8	63.0	58.7	54.5

Table 4. Similar PK parameters of single cell- and *in vitro*-assembled TDBs in cynos. The PK data were characterized with NCA. Actual dose concentrations were used in data analysis (see Material and Methods). Standard error values for each parameter are provided. C_{max} = Maximum observed serum concentration, AUC_{0-4} = Area under the serum-concentration time curve from time 0 to day 4.

PK parameter	Anti-FcRH5/CD3 TDB		
	<i>In vitro</i> -assembled (n = 4)	Single cell v10 (n = 4)	Single cell v11 (n = 4)
Actual dose (mg/kg)	2.12	1.96	1.94
C_{max} ($\mu\text{g/mL}$)	46.6 \pm 4.31	41.8 \pm 3.66	36.6 \pm 4.02
C_{max}/Dose ($\mu\text{g/mL}/(\text{mg/kg})$)	22.0 \pm 2.03	18.7 \pm 2.05	21.6 \pm 1.88
AUC_{0-4} (day- $\mu\text{g/mL}$)	43.7 \pm 9.65	41.2 \pm 4.70	37.2 \pm 9.43
AUC_{0-4}/Dose (day- $\mu\text{g/mL}/(\text{mg/kg})$)	20.7 \pm 4.55	19.0 \pm 4.78	21.2 \pm 2.42

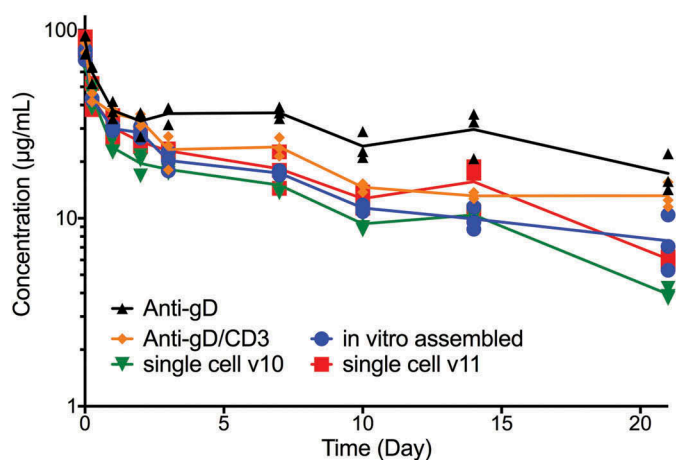


Figure 3. Similar PK profiles of single cell and *in vitro*-assembled TDBs following single dose (5 mg/kg) IV administration to C.B-17 SCID mice (n = 3, at each time point). Individual data points (symbols) are shown together with mean values connected (solid lines). Controls included monospecific (anti-gD) or bispecific (anti-gD/CD3) antibody. Blue circles denote *in vitro*-assembled TDB, green reverse triangles denote single cell TDB v10, red squares denote single cell TDB v11, black triangles denote anti-gD and orange diamond denote anti-gD/CD. Associated two-compartment model profiles are shown in Fig. S3.

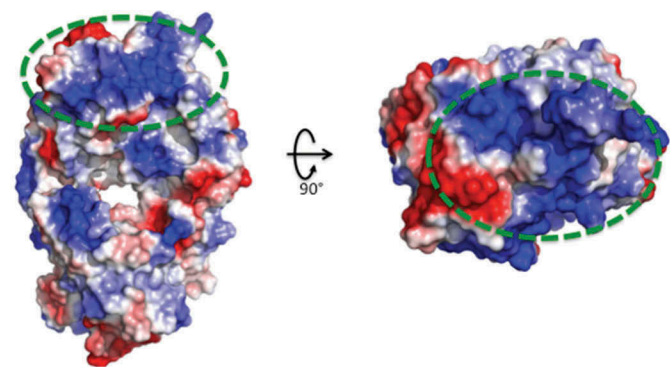


Figure 4. The structure of the anti-CD3 arm Fab from the side and the top show the exposed positive charges on the Fab. The molecular surface rendering is color coded by electrostatic potential: positively charged (blue), negatively charged (red) or neutral (white). The structure on the left shows the Fab fragment from the side, and the structure on the right shows the Fab arm from the top. The curved arrow points in the direction of the rotation of the structure from the side to the top. The green dashed circle denotes the antigen-binding region on the anti-CD3 arm Fab and the exposed positively charged surface (blue) on the anti-CD3 Fab on both.

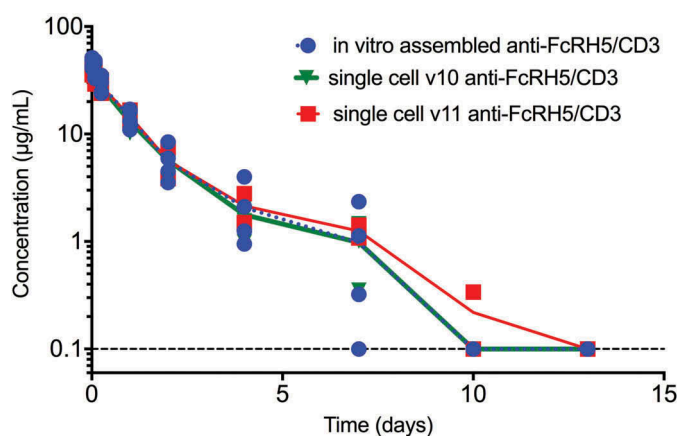


Figure 5. Similar PK profiles of single cell and *in vitro*-assembled TDBs following single dose (2 mg/kg) IV infusion administered to cynos (n = 4). Individual data points (symbols) are shown together with mean values connected (solid lines). Blue circles denote *in vitro*-assembled TDBs, green reverse triangles denote single cell TDBs v10, red squares denote single cell TDB v11. The serum-concentration time profiles are limited to the first 13 days, after which values were below LLOQ. Associated ADA data are shown in Fig. S5.

The PK profiles of the single cell TDBs overlapped with the PK profile of the *in vitro*-assembled TDB (Figure 5). All the concentrations were below the limit of quantification by day 13 for animals administered anti-FcRH5 TDBs, which could be due to ADA or antigen-mediated clearance of the antibodies. The nominal and dose-normalized mean C_{max} and AUC_{0-4} values were comparable across the 3 TDB groups (Table 4).

In addition, we conducted two-compartment model fitting for cyno PK. Because ADA was detected as early as day 7, we analyzed the PK profiles until day 4. While we obtained relatively good fits for individual profiles, the standard error values for parameters V_p and CL_D were rather high for some of the subjects (data not shown). The two-compartment model analysis could not accurately estimate these parameters and resulted in high standard error values due to limited data points up to only day 4.

Single cell and *in vitro*-assembled anti-FcRH5/CD3 TDBs showed consistent PD activity in cynos

A decrease of FcRH5-expressing cells in cynos is the primary PD endpoint for the anti-FcRH5/CD3 TDBs.¹¹ Therefore, we measured PCs and B cells in BM, as well as B cells in blood, to evaluate the PD activity of the three TDBs in cynos administered a single dose of 2 mg/kg (Figure 6 and Fig. S5). In addition, we measured serum IgG as a secondary endpoint resulting from PC depletion.¹¹ We also measured T-cell activation (Figure 7(a,b)), relevant cytokine levels (i.e., interleukin (IL)-6 and interferon (IFN)- γ) (Figure 7(c,d)), and T cell counts in circulation (Fig. S6), which are all relevant PD endpoints associated with anti-FcRH5/CD3 TDB MOA.¹¹

All TDB-administered groups exhibited robust PC and B cell decreases in cyno BM on day 7 (Figure 6(a,b) that was followed by a trend towards recovery on day 22 and full recovery by day 55 (Fig. S6A-D). Serum B cell counts decreased immediately in all animals following TDB administration (Figure 6(d)). B-cell counts remained at minimal

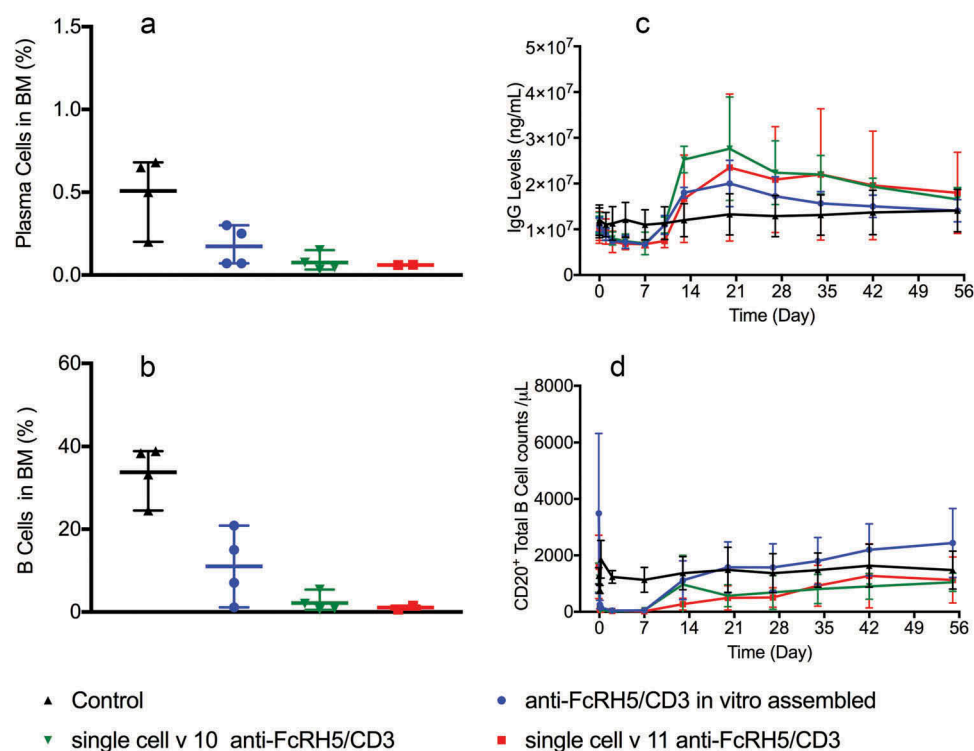


Figure 6. Single cell and *in vitro*-assembled TDBs have similar *in vivo* PD activity. Black triangles denote control group, blue circles denote *in vitro*-assembled TDB group, green reverse triangles denote single cell TDB v10 group, red squares denote single cell TDB v11 group. (a) PC % values at day 7 for single cell and *in vitro*-assembled TDBs along with control group. Individual data points are presented in addition to the mean values and max-min ranges for each group. Mean and standard values are the following: control group (0.5% ± 0.22%), *in vitro*-assembled TDB group (0.17% ± 0.12%), single cell TDB v10 (0.07% ± 0.053%), single cell produced TDB v11 (0.06% ± 0.00%). (b) B Cell % values at day 7 for single cell and *in vitro*-assembled TDBs along with control group. Individual data points are presented in addition to the mean values and max-min ranges for each group. Mean and standard values as follows: control group (33.8% ± 6.7%), *in vitro*-assembled TDB group (11.0% ± 8.7%), single cell TDB v10 group (2.17% ± 2.23%), single cell TDB v11 (1.05% ± 0.63%). (c) IgG serum concentration-time profiles for single cell and *in vitro*-assembled TDBs along with control group. Data are presented as connected mean values (solid lines) for each group throughout the study. The error bars represent the standard deviations at each time point. All the TDB administered groups followed similar profiles while the control group profile remained flat throughout the study. (d) B cell counts – time profiles for single cell and *in vitro*-assembled TDBs along with control group. Data are presented as connected mean values (solid lines) for each group throughout the study. The error bars represent the standard deviations at each time point. All the TDB administered groups followed similar profiles whereas the control group profile remained relatively flat throughout the study.

levels up to day 7 and exhibited a gradual increase starting at day 14 until the end of the study (Figure 6(d)) for all TDB-administered groups.

We observed an initial decrease in serum IgG levels up to day 7 in all TDB-administered groups (Figure 6(c)). After day 7 serum IgG levels increased up to day 22 (Figure 6(c)), before returning to baseline in all TDB-administered animals by the end of the study.

All TDB-administered groups exhibited transient T-cell activation (Figure 7(a,b) and cytokine level changes (IL-6 and IFN- γ) (Figure 7(c,d)) returning to baseline within 24 hours. Lastly, all the groups treated with TDB exhibited an immediate and transient decrease in T cell counts following TDB administration (Fig. S6). T cell counts increased up to 14 days above their baseline and returned to baseline at the end of the study.

Discussion

In this study, we compared single cell anti-FcRH5/CD3 TDBs (v10 and v11) to *in vitro*-assembled anti-FcRH5/CD3 TDB using comprehensive *in vitro* and *in vivo* PK/PD assessments. Pharmacological performance of two single cell bispecific designs was tested in a binding animal species (cyno). This

study showed for the first time that cyno PK/PD behaviors of the single cell TDBs were pharmacologically comparable to *in vitro*-assembled TDB. In addition, we evaluated recovery profiles of anti-FcRH5/CD3 TDB-dependent PD changes, such as PC and B cell decreases and serum IgG levels in cynos beyond 7 days. Our results showed that PD changes mediated by anti-FcRH5/CD3 TDB were reversible, and that the recovery profiles agreed with the expected MOA of the TDB.

Single cell TDBs and *in vitro*-assembled TDB had comparable binding to both FcRH5 and CD3 antigens. In addition, all three TDBs showed robust and consistent *in vitro* cytotoxic activity of cyno and human PCs, MOLP-2 cell line, as well as T-cell activation. We observed slightly higher T-cell activation (Figure 2(d)) for the single cell TDBs compared to *in vitro*-assembled TDB, but this difference did not translate to any differences in MOLP-2 cell line cytotoxic activity. We did not observe 100% cell killing in *in vitro* experiments, consistent with observations for other TDBs.^{12,26} While the exact cause of incomplete *in vitro* cell killing is unknown, one possible explanation is the variability in the relative numbers of effector cells and expression levels of target cells from different donors since the killing activity of TDBs depend on both of these parameters. One limitation of these results was the small

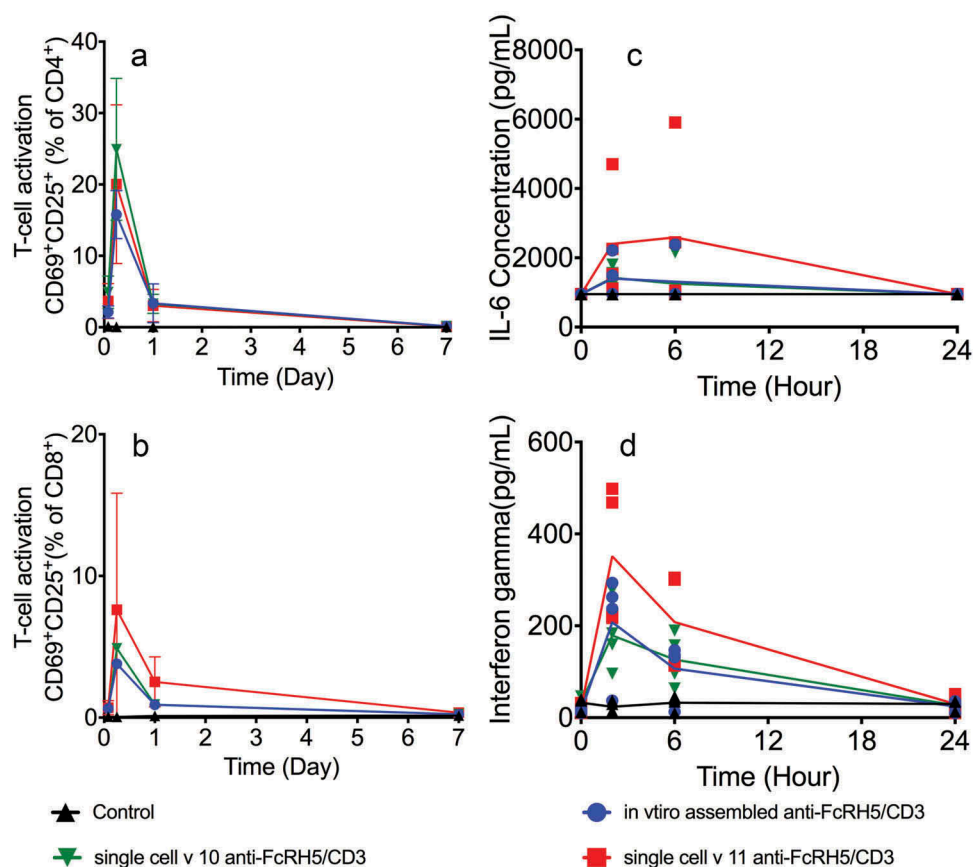


Figure 7. Single cell- and *in vitro*-assembled TDBs had similar *in vivo* T-cell activation and cytokine profiles in cynos. Black triangles denote control group, blue circles denote *in vitro*-assembled TDB group, green reverse triangles denote single cell TDB v10 group, red squares denote single cell TDB v11 group. (A-B) T-cell activation-time profiles for single cell and *in vitro*-assembled TDBs. Data are presented as connected mean values (solid lines) for each group throughout the study. The error bars represent the standard deviations at each time point. All the TDB administered groups followed similar profiles whereas the control group profile remained flat throughout the study. (a) CD4⁺ T-cell activation-time profile for single cell and *in vitro*-assembled TDBs. (b) CD8⁺ T-cell activation-time profile for single cell and *in vitro*-assembled TDBs. (c, d) Cytokine concentration-time profiles for single cell and *in vitro*-assembled TDBs. Individual data points are presented (as symbols) in addition to connected mean values (solid lines) for each group throughout the study. All the TDB administered groups followed similar profiles whereas the control group profile remained flat throughout the study. (c) IL-6 serum concentration-time profiles (d) IFN- γ serum concentration-time profiles.

sample size and the low number of donors used in the *in vitro* studies. However, we still confirmed *in vitro* activity of the single cell TDBs and that there were no major differences between single cell TDBs and the *in vitro*-assembled TDB before proceeding to *in vivo* PK/PD studies.

The mouse (non-binding species) PK study was conducted to identify any issues with target-independent PK of single cell TDBs before evaluating the PK/PD in cynos (binding species). We selected an immune-deficient mouse strain, SCID.bg mice, to avoid any potential ADA impact on the exposure of the TDBs. The observed variability in the PK profiles was likely due to sparse sampling, where the samples were collected from different mice at different time points and the samples were pooled to get the full PK profile for each group. The exposures of the single cell TDBs were comparable to the exposure of the *in vitro*-assembled TDB in SCID.bg mice. Furthermore, all anti-FcRH5/CD3 TDBs showed lower exposure compared to anti-gD in SCID.CD17 mice. Interestingly, the anti-gD/CD3 bispecific antibody also appeared to clear more rapidly than the anti-gD antibody, suggesting that the lower exposure of the three TDBs was likely due to the anti-CD3 arm. Therefore, we explored whether physicochemical properties of the CD3 arm contributed, non-specifically, to

the observed lower exposure. iCAT evaluation suggested that anti-CD3 had a higher than acceptable Fv charge. One limitation of using iCAT to estimate Fv charge is that this tool was developed for bivalent, rather than bispecific, molecules to assess their risk for fast clearance in cynos.²⁵ We also examined the structure of the anti-CD3 arm Fab region. A positive charge patch has been shown to increase the non-specific clearance of bivalent antibodies.^{27–29} Together these findings suggest that positive charge patches on the anti-CD3 arm could have potentially contributed to the lower exposures of both FcRH5/CD3 and anti-gD/CD3 compared to the bivalent anti-gD without a CD3 arm.

It is generally assumed that exposure drives biological activity for protein therapeutics; hence, comparison of PK alone has been considered an adequate measure for evaluating the differences in *in vivo* behavior of a molecule.³⁰ *In vitro*-assembled anti-FcRH5/CD3 TDB exhibited similar PK behavior when compared with the previous cyno study.¹¹ We included the PD endpoint evaluation in this cyno study due to the steep dose response observed in PC depletion with the anti-FcRH5/CD3 TDB in the previous cyno study.¹¹ In that study, depletion of PCs following anti-FcRH5/CD3 TDB treatment was observed in cynos treated with doses of 2 mg/

kg or higher, while doses of 1 mg/kg resulted in incomplete PC depletion.¹¹ Since anti-FcRH5/CD3 TDB was well tolerated at 1, 2 and 4 mg/kg in the cynos,¹¹ we initially considered conducting the study at 4 mg/kg, which was the highest tested dose. However, conducting the study at 4 mg/kg would mean that the comparison would have been on the plateau of the dose-response curve, and any potential differences would not be captured. Hence, we chose a 2 mg/kg dose so that PC depletion information could identify pharmacological differences, if any, between single cell TDBs and *in vitro*-assembled TDB. Single cell TDBs and *in vitro*-assembled TDB exhibited robust PC and B cell killing, T-cell activation and cytokine level increases in cynos. In addition to PK/PD of single cell TDBs, immunogenicity of the single cell TDBs was also assessed, and no differences were observed when compared to immunogenicity of the *in vitro*-assembled TDB.

In addition, we evaluated the recovery of anti-FcRH5/CD3-dependent PD changes. After being produced in BM, B cells migrate to other secondary lymphoid tissues through circulation where they mature and differentiate. Our results showed that B cells recovered fully in BM within 55 days after a single dose of the TDBs. Similarly, B cell counts in peripheral blood exhibited a comparable recovery rate to B cells in BM. The observed recovery rate of B cells in BM and blood is consistent with the B cell proliferation rate of ~2% per day, which corresponds to ~50 day lifespan in cynos.³¹

We expected a similar correlation between PCs and IgG levels such that PCs in BM and IgG levels in blood would follow similar recovery patterns.³² However, our results showed IgG levels decreased for the first 7 days, and then increased above baseline levels until day 22 before returning to the baseline. The PCs in the BM in TDB-treated groups were not higher than the PCs in the control group at day 22. The mechanism underlying the substantial rebound of IgG levels around day 22 is not entirely understood. We may have missed a rebound effect in BM PCs due to constraints with BM aspirate sampling (i.e., collections can only be done weekly in cynos), making it difficult to show correlations between BM PCs and IgG levels in circulation. An alternative hypothesis is that available B cells in circulation (B cell numbers in circulation increased after day 7) and plasmablasts may overproduce IgGs to reach homeostasis and to compensate for IgG depletion as quickly as possible. The presence of ADA may have also contributed to total IgG levels, as likely ADA-producing B cells increased in number after day 7.

Both IgG levels and B cells in circulation started increasing after day 7 when the concentration of anti-FcRH5 TDB was below ~1 µg/mL. We have insufficient data to draw any quantitative conclusions on the relationship between anti-FcRH5/CD3 TDB concentration and IgG levels or PCs in BM. However, it is possible that maintaining a certain level of exposure of anti-FcRH5/CD3 TDB in circulation might prevent the increase of IgG levels and/or PCs. Further PK/PD studies combined with a computational modeling analysis will be needed to fully understand these relationships.

TDBs have the potential of a longer half-life in human compared to smaller size formats such as blinatumomab due to the presence of the Fc region, which confers the advantage of FcRn recycling similar to monoclonal antibodies.³³

In summary, we compared single cell TDBs to *in vitro*-assembled TDBs qualitatively using comprehensive *in vitro* and *in vivo* PK/PD analyses. In addition to similar *in vitro* properties and mouse PK, the single cell TDBs exhibited similar PK/PD behavior and immunogenicity to *in vitro*-assembled TDB in cynos, which is the relevant preclinical species for anti-FcRH5/CD3 TDBs. We also showed that anti-FcRH5/CD3 TDB-mediated PD changes were reversible, and that the recovery profiles agreed with the TDB MOA. Overall, our study supports further development of the single cell anti-FcRH5/CD3 TDBs and other future single cell bispecific programs. Single cell production of single cell bispecifics will facilitate a faster and simpler production process in addition to being more cost efficient. As a result, this offers an overall effective production process for bispecific antibodies.

Materials and methods

Ethics statement

The authors confirm that they have obtained appropriate institutional review board, in Genentech and in Covance, approval for all animal experimental investigations.

Production of test materials

Anti-CD3ε and anti-FcRH5 antibodies are humanized hybridoma antibodies obtained from mice immunized with their respective antigens. *In vitro*-assembled anti-FcRH5/CD3 was produced as previously described.¹¹ In brief, the knob (T366W) and hole (T366S, L368A, Y407V) half-antibodies were expressed in separate Chinese hamster ovary cells to ensure cognate light chain pairing and purified via Protein A affinity chromatography.^{13–15,34} Equal amounts of the two half-antibodies were incubated with a 200-fold molar excess of reduced glutathione at pH 8.5 overnight at 32°C to facilitate formation of the inter-heavy chain disulfide bonds. The assembled bispecific antibody was purified from contaminants through hydrophobic interaction chromatography.

Single cell bispecific designs included amino acid changes in the Fab variable region, outside of the CDRs and the constant domains in conjunction with previously described KIH mutations.¹⁴ Anti-FcRH5/CD3 single cell design v10 and anti-FcRH5/CD3 single cell design v11 were produced as previously described.¹⁸ The control IgG was anti-gD, targeting the glycoprotein D epitope of herpes simplex virus, and was produced in Genentech.

Radioligand cell binding assay for human and cyno FcRH5 affinity measurement

The three anti-FcRH5/CD3 variants were iodinated using the Iodogen method.³⁵ In a competition reaction, serially-diluted unlabeled antibody was mixed with a fixed concentration of corresponding iodinated antibody in 96-well plates. The final concentration of the unlabeled antibody started at 500 nM, followed by eleven 3-fold dilutions. One reaction was performed without the addition of any unlabeled antibody. Stably transfected SVT2 (SV40-transformed mouse fibroblast cells) cell lines expressing human FcRH5 or cyno FcRH5 were detached from the flasks using cell dissociation solution (Sigma-Aldrich, C5914), washed with binding a buffer, and added to the competition reaction in the 96-well plates. The competition reactions with cells were assayed

in triplicate for each concentration of unlabeled antibody and incubated for 2 h at room temperature. After the 2 h incubation at room temperature, the competition reactions were washed 4 times with binding buffer to remove the unbound iodinated antibody. The air-dried filters were counted on a Wallac Wizard 2470 gamma counter (PerkinElmer Life and Analytical Sciences) and the binding data were evaluated using NewLigand software (Genentech), which uses the fitting algorithm of Munson and Rodbard to determine the K_D of the antibody.³⁶

Affinity measurement by SPR for human and cyno CD3 ϵ antigen

Kinetic interactions were measured by SPR on a Biacore T200 instrument. Using a Series S CM5 chip, soluble recombinant CD3 ϵ antigen was immobilized by means of amine coupling. Immobilization levels were between 200 and 250 RU for each of the 3 test flow cells (2, 3 and 4). Flow cell 1 was activated and blocked as for active flow cells without antigen present to be used as control. Each antibody construct flowed over the chip in a concentration series ranging from 0.05–50 nM. Measurements were taken at 25°C at a flow rate of 30 μ L/min in 10 mM HEPES, pH 7.4, 150 mM NaCl, 0.05% Tween 20 (HBSP) running buffer. Kinetic information was calculated by fitting data to a 1:1 binding model. Reference subtraction and data fitting were performed using BIAevaluation software (GE Life Sciences).

Antibody variable region (Fv) charge and hydrophobicity

In silico clearance assessment tool (iCAT) is a sequence-based calculation tool that provides a theoretical risk assessment of antibody clearance in cynos.²⁵ This assessment is based on theoretical parameters extracted from the Fv domain sequence. The iCAT score was evaluated for the anti-CD3 bivalent antibody.

In vitro cytotoxicity assay for cyno PCs and human donor PCs

A cyno BM aspirate sample ($n = 1$, male) was procured from BioreclamationIVT. BMMCs were isolated from the cyno BM aspirate by lysing the red blood cells twice with ACK red cell lysis buffer for 10 min at room temperature upon arrival at Genentech. Cyno BMMCs were incubated for 72 h at 37°C with various concentrations of the 3 anti-FcRH5/CD3 TDB variants. The cyno PC were classified by flow cytometry as CD45⁻CD20⁻CD38⁺PC⁺.³⁷ The killing activity was calculated as follows: 100 (number of live target cells without TDB – number of live target cells with TDB)/number of live target cells without TDB.

Human BM aspirates from healthy donors ($n = 2$, male) (procured from AllCells, ABM001-1) were diluted in phosphate-buffered saline and BMMCs were isolated by conventional gradient separation. BMMCs were incubated for 72 h at 37°C with various concentrations of anti-FcRH5/CD3 variants. Cells were stained for cell surface markers to define PC and propidium iodide (PI) was added to the final cell suspension. The number of live PC was assessed by flow cytometry using a gate of CD38⁺CD138⁺PI⁻. The killing activity was calculated as described above.

Determination of concentration- cell killing percentage data was undertaken in duplicate. The data were fitted to sigmoidal E_{max} model, where the Hill coefficient was equal to 1, in GraphPad Prism 7°. Concentration- cell killing percentage data were characterized with two parameters; E_{max} and EC_{50} .

In vitro cell killing assay in MOLP-2 cells and T-cell activation

MOLP-2 is a MM cell line that expresses FcRH5 at a level similar to that found on MM tumor cells.¹¹ MOLP-2 cells were labeled with carboxyfluorescein succinimidyl ester (CFSE; ThermoFisher Scientific) following the manufacturer's instructions. Human peripheral blood mononuclear cells (PBMCs) were isolated from whole blood of healthy donors ($n = 3$) by Ficoll gradient.

Human CD8⁺ T cells were isolated from PBMCs using a human CD8⁺ T cell Isolation Kit (Miltenyi Biotec, 130–096–495). Human CD8⁺ T cell and MOLP-2 cells (3:1 ratio) were incubated in the presence of various concentrations of the 3 anti-FcRH5/CD3 variants for either 24 h (T-cell activation) or 48 h (MOLP-2 cell killing). After incubation, PI was added to the final cell suspension. The number of live MOLP-2 cells was assessed by flow cytometry using a gate for CFSE⁺PI⁻. The killing activity was calculated as described above. Concentration- MOLP-2 cell killing percentage data were collected in duplicate. The data were fitted to a sigmoidal E_{max} model, where the Hill coefficient was equal to 1, in GraphPad Prism 7°. Concentration- MOLP-2 cell killing percentage data were characterized with two parameters; E_{max} and EC_{50} .

For CD8⁺ T-cell activation, cells were stained with anti-CD8-FITC, anti-CD69-PE, and anti-CD25-APC. CD69 and CD25 surface expression was detected on CD8⁺ T cells by flow cytometry. The percentage of CD8⁺ T cells that were CD69⁺CD25⁺ were reported.

Concentration- T-cell activation percentage data were undertaken in duplicate. The data were fitted to a sigmoidal E_{max} model, where the Hill coefficient was equal to 1, in GraphPad Prism 7°. Concentration- T-cell activation percentage data were characterized with 2 parameters, E_{max} and EC_{50} .

PK of single cell and in vitro-assembled anti-FcRH5/CD3 TDBs in CB-17. SCID mice

This study was designed to evaluate and compare the PK of three anti-FcRH5/CD3 TDB variants. Anti-gD and anti-gD/CD3 were also included as control antibodies. Five groups of female CB-17.SCID mice ($n = 9$ per group; Charles River Laboratories, 251) were administered a single IV dose of each antibody at a dose of 5 mg/kg. The number of animals was chosen to collect 3 samples per time point with a sparse sampling so that basic descriptive statistics could be obtained.

Female mice were used for convenience. Historically, we have not observed any differences in PK studies that used male or female mice. Blood samples were collected via the femoral vein at selected time points (3 replicates for each time point) for up to 21 days. Total antibody concentrations in serum were determined by a GRIP ELISA (plate coated with anti-human IgG and detected with anti-human IgG) with the limit of detection of 15.6 ng/mL and used for PK evaluations. The dosing solution recoveries were 88%, 114%, 101%, 93%

and 130%, for anti-gD, anti-gD/CD3, anti-FcRH5/CD3 *in vitro*-assembled, anti-FcRH5/CD3 v10 and anti-FcRH5/CD3 v11, respectively. The PK profiles were pooled from different mice at different time points. Nominal sample collection times and actual dose solution concentrations were used in data analysis. NCA parameters were estimated using Phoenix WinNonlin® 64 with sparse sampling and IV bolus input. Two-compartment model parameters were estimated using Simbiology® in MATLAB® 2016a with the combined error model described in the software. Standard error values were provided for both analyses. Mice were euthanized after being anesthetized with isoflurane (5% isoflurane with 2 L/min of O₂). All procedures were approved by and conformed to the guidelines and principles set by the Institutional Animal Care and Use Committee (IACUC) of Genentech and were performed in a facility accredited by Association for Assessment and Accreditation of Laboratory Animal Care International.

PK/PD of single cell and *in vitro*-assembled anti-FcRH5/CD3 tdb in cynos

The PK and PD properties of three anti-FcRH5/CD3 TDB variants were evaluated in naive, male cynos at Covance, Madison. Cynos were administered a single-dose, 2 mg/kg IV infusion (1 h) of each test article (single cell v10, single cell v11 and *in vitro*-assembled TDB) and vehicle (n = 4 per group). The vehicle control article was 20 mM histidine chloride, 240 mM sucrose, 0.02% v/v Tween 20 in sterile water. Male cynos were used for consistency with the previous published cyno study.¹¹ Blood samples were collected by venipuncture via the femoral vein pre-study and at pre-dose and selected time points for 55 days after dosing for analyses of hematology, serum chemistry, coagulation, and PK and PD endpoints (cytokines, flow cytometry of T lymphocytes, B lymphocytes, activated T lymphocytes and cyno serum IgG).

BM was collected from anesthetized animals by aspiration from the humerus pre-study and on days 7, 22 and 55 for evaluation of B lymphocytes and PC by flow cytometry. The study was terminated at day 55. All the surviving animals were returned to the colony. All procedures were approved by the Covance IACUC and were performed in compliance with the Animal Welfare Act, the Guide for the Care and Use of Laboratory Animals, and the Office of Laboratory Animal welfare.

The number of animals chosen for this study was limited by ethical concerns. Previously, we used 3 cynos per group and demonstrated clear PC depletion compared to a control group at 2 mg/kg when dosed with *in vitro*-assembled TDB.¹¹ In this cyno study, we used 4 cynos per group and dosed the animals with 2 mg/kg of single cell or *in vitro*-assembled TDBs. Our expectation was that, if the single cell TDBs were pharmacologically comparable to *in vitro*-assembled TDB, we would observe clear PC depletion in the single cell TDB dosed groups compared to the control group at 2 mg/kg.

PK assay evaluation in cyno

High-performance liquid chromatography with mass spectrometry (MS)/MS detection (multiple reaction monitoring) was used to quantify the total form of the three anti-FcRH5/CD3

variants in cyno sera. An affinity capture approach using streptavidin magnetic beads coated with biotinylated anti-HuIgG antibody (Clone R10Z, Genentech) was used to enrich anti-FcRH5/CD3 in serum. Three characteristic tryptic peptides, derived from the heavy chain region and light chain region, were selected for monitoring in the assay as surrogates of the total antibody concentration originating from anti-FcRH5/CD3. The method is applicable to the quantitation of anti-FcRH5/CD3 within a nominal range of 100–25,000 ng/mL. The lower limit of quantification (LLOQ) is nominally 100 ng/mL.

NCA parameters were estimated using Simbiology®, in MATLAB® 2016b with IV infusion input. The dosing solution recoveries were 106%, 97% and 98% for anti-FcRH5/CD3 *in vitro*-assembled, anti-FcRH5/CD3 v10 and anti-FcRH5/CD3 v11, respectively. Nominal sample collection times and actual dose solution concentrations were used in data analysis. All PK analysis was based on individual animal data.

Flow cytometric assessment of cyno BM PCs and B cells

Cyno BM aspirates were diluted (1:10) into ammonium chloride-potassium chloride buffer to lyse the red blood cells. All antibodies for cell staining were from BD Biosciences unless otherwise indicated. Cyno BM cells were stained with anti-CD45-V500 (sc-53,665, Santa Cruz Biotechnology), anti-CD20-PE (sc-7733, Santa Cruz Biotechnology), and anti-CD38-AF647 (sc-374,650, Santa Cruz Biotechnology) using the manufacturer's recommended volumes for the antibodies. The cyno PC were identified by flow cytometry as those cells that were CD45⁻CD20⁻CD38⁺PC⁺. Depletion of B cells in BM was evaluated by the percentage of CD45⁺CD20⁺ in CD45⁺ cells.

ADA detection in cyno

A generic immune-complex immunoassay was used to screen cyno serum samples for anti-drug antibodies as described elsewhere.³⁸ In this assay, baseline and post-baseline samples from each animal were diluted and incubated with anti-FcRH5/CD3 variants, to allow formation of any ADA-drug complex. A mouse anti-human Fc- antibody (R10Z8E9, Genentech) immobilized on 96-well microtiter plates captured the ADA/therapeutic immune-complexes. A horseradish peroxidase (HRP)-labeled goat anti-monkey IgG (H + L) antibody (sc-2458, Santa Cruz Biotechnology) was used for detection. The relative sensitivity of the assay in neat serum, estimated using the positive control (human IgG and cyno IgG fusion) was approximately 40.7 ng/mL. The assay could detect 1,000 ng/mL of affinity-purified cyno anti-HuIgG antibodies in the presence of 440 µg/mL of a monoclonal antibody-derived molecule.

IgG levels in cyno

Samples and QCs containing IgG were bound to the immobilized anti-monkey IgG, and detected using goat anti-monkey IgG conjugated to HRP (sc-2458, Santa Cruz Biotechnology). A standard curve was manually prepared fresh on the day of use in sample diluent using protein A purified cyno IgG. The calibration standards ranged from 6.25 to 800 ng/mL (in-well concentrations). Study samples were diluted to the minimum

required dilution (MRD) of 1/150,000 in sample diluent. The sensitivity of the assay (LLOQ) was 6.25 ng/mL. SoftMax Pro 6.3 with 4PL curve fit with 1/y weighting was used for regression of calibration curve and data analysis.

Flow cytometric assessment of cyno blood

The relative percentages of each phenotype obtained from the flow cytometer were multiplied by the absolute lymphocyte count from the hematology analysis in order to enumerate absolute cell counts. The following lymphocyte subsets were quantitated using flow cytometry: B cells (CD4⁻CD8⁻CD20⁺), CD4 cells (CD4⁺CD8⁻), CD8 cells (CD4⁻CD8⁺CD16⁻), CD25⁺CD69⁺ expressing CD4⁺ T cells (CD4⁺CD8⁻CD25⁺CD69⁺), CD25⁺CD69⁺, and CD25⁺CD69⁺ expressing CD8⁺ T cells (CD4⁻CD8⁺CD16⁻CD25⁺CD69⁺). The percentages of CD8⁺ and CD4⁺ T cells that were CD69⁺CD25⁺ were reported as T-cell activation.

Cytokine levels in cynos

Plasma samples were analyzed for selected cytokines on the Milliplex MAP NHP Cytokine Magnetic Bead Panel Kit in Plasma using a method validated at Covance Greenfield. Cytokine levels were similar to values reported previously.¹¹ Therefore, only IL-6 and INF- γ levels are presented here.

Abbreviations

ADA	anti-drug antibodies
AUC	area-under-the-curve
BM	bone marrow
BMMC	bone marrow mononuclear cell
CDR	complementarity-determining region
cynos	cynomolgus monkeys
Fc	fragment crystallizable
FcRH5	Fc receptor-like protein 5
Fv	antibody variable fragment
iCAT	<i>in silico</i> clearance assessment tool
IV	Intravenous
KIH	knobs-into-holes
LLOQ	lower limit of quantification
MM	multiple myeloma
MOA	mechanism of action
NCA	non-compartmental analysis
PBMC	peripheral blood mononuclear cell
PC	plasma cells
PD	pharmacodynamics
PK	pharmacokinetics
SPR	surface plasmon resonance
TDB	T cell-dependent bispecific

Acknowledgments

We thank Crystal Zhang, Sheila Ulufatu and Christopher Stevenson for the mouse study. We thank Pamela Chan for assistance with the anti-FcRH5/CD3 GRIP ELISA.

Disclosure statement

All authors are current or former employees of Genentech, Inc., a member of the Roche Group, and may hold stock and options. This work was funded and conducted by Genentech, Inc.

ORCID

Nicola Stagg  <http://orcid.org/0000-0002-1082-6768>
 Diego Ellerman  <http://orcid.org/0000-0002-3056-3600>
 Trung Nguy  <http://orcid.org/0000-0002-0171-2873>
 Weiru Wang  <http://orcid.org/0000-0001-8845-301X>
 Jochen Brumm  <http://orcid.org/0000-0001-9518-038X>
 Kedan Lin  <http://orcid.org/0000-0003-0144-6883>
 Paul J. Carter  <http://orcid.org/0000-0001-7854-062X>
 Christoph Spiess  <http://orcid.org/0000-0002-0570-9700>

References

- Eslick R, Talaulikar D. Multiple myeloma: from diagnosis to treatment. *Aust Fam Physician*. 2013;42:684–688.
- Zannetti BA, Tacchetti P, Pantani L, Gamberi B, Tosi P, Rocchi S, Cellini C, Ronconi S, Pezzi A, Mancuso K, et al. Novel agent-based salvage autologous stem cell transplantation for relapsed multiple myeloma. *Ann Hematol*. 2017; doi: 10.1007/s00277-017-3140-5.
- Kuroda J. Therapeutic approach for relapsed/refractory multiple myeloma: the logic and practice. *Rinsho Ketsueki*. 2017;58:2058–2066. doi:10.11406/rinketsu.58.2058.
- Dingli D, Ailawadhi S, Bergsagel PL, Buadi FK, Dispenzieri A, Fonseca R, Gertz MA, Gonsalves WI, Hayman SR, Kapoor P, et al. Therapy for relapsed multiple myeloma: guidelines from the mayo stratification for myeloma and risk-adapted therapy. *Mayo Clin Proc*. 2017;92:578–598. doi:10.1016/j.mayocp.2017.01.003.
- Kantarjian H, Stein A, Gokbuget N, Fielding AK, Schuh AC, Ribera JM, Wei A, Dombret H, Foà R, Bassan R, et al. Blinatumomab versus chemotherapy for advanced acute lymphoblastic leukemia. *N Engl J Med*. 2017;376:836–847. doi:10.1056/NEJMoa1609783.
- Ghione P, Moskowitz AJ, De Paola NEK, Horwitz SM, Ruella M. Novel Immunotherapies for T Cell Lymphoma and Leukemia. *Curr Hematol Malig Rep*. 2018; doi: 10.1007/s11899-018-0480-8.
- June CH, Sadelain M. Chimeric antigen receptor therapy. *N Engl J Med*. 2018;379:64–73. doi:10.1056/NEJMra1706169.
- Yu S, Li A, Liu Q, Yuan X, Xu H, Jiao D, Pestell RG, Han X, Wu K. Recent advances of bispecific antibodies in solid tumors. *J Hematol Oncol*. 2017;10:155. doi:10.1186/s13045-017-0522-z.
- Dahlen E, Veitonmaki N, Norlen P. Bispecific antibodies in cancer immunotherapy. *Ther Adv Vaccines Immunother*. 2018;6:3–17. doi:10.1177/2515135518763280.
- Runcie K, Budman DR, John V, Seetharamu N. Bi-specific and tri-specific antibodies- the next big thing in solid tumor therapeutics. *Mol Med*. 2018;24:50. doi:10.1186/s10020-018-0051-4.
- Li J, Stagg NJ, Johnston J, Harris MJ, Menzies SA, DiCara D, Clark V, Hristopoulos M, Cook R, Slaga D, et al. Membrane-Proximal epitope facilitates efficient T Cell synapse formation by Anti-FcRH5/CD3 and Is a requirement for myeloma cell killing. *Cancer Cell*. 2017;31:383–395. doi:10.1016/j.ccell.2017.02.001.
- Junttila TT, Li J, Johnston J, Hristopoulos M, Clark R, Ellerman D, Wang BE, Li Y, Mathieu M, Li G, et al. Antitumor efficacy of a bispecific antibody that targets HER2 and activates T cells. *Cancer Res*. 2014;74:5561–5571. doi:10.1158/0008-5472.CAN-13-3622-T.
- Ridgway JB, Presta LG, Carter P. ‘Knobs-into-holes’ engineering of antibody CH3 domains for heavy chain heterodimerization. *Protein Eng*. 1996;9:617–621.
- Atwell S, Ridgway JB, Wells JA, Carter P. Stable heterodimers from remodeling the domain interface of a homodimer using a phage display library. *J Mol Biol*. 1997;270:26–35. doi:10.1006/jmbi.1997.1116.
- Spiess C, Merchant M, Huang A, Zheng Z, Yang NY, Peng J, Ellerman D, Shatz W, Reilly D, Yansura DG, et al. Bispecific antibodies with natural architecture produced by co-culture of bacteria expressing two distinct half-antibodies. *Nat Biotechnol*. 2013;31:753–758. doi:10.1038/nbt.2621.

16. Kamath AV, Lu D, Gupta P, Jin D, Xiang H, Wong A, Leddy C, Crocker L, Schaefer G, Sliwkowski MX, et al. Preclinical pharmacokinetics of MEHD7945A, a novel EGFR/HER3 dual-action antibody, and prediction of its human pharmacokinetics and efficacious clinical dose. *Cancer Chemother Pharmacol*. 2012;69:1063–1069. doi:10.1007/s00280-011-1806-6.
17. Yu YJ, Zhang Y, Kenrick M, Hoyte K, Luk W, Lu Y, Atwal J, Elliott JM, Prabhu S, Watts RJ, et al. Boosting brain uptake of a therapeutic antibody by reducing its affinity for a transcytosis target. *Sci Transl Med*. 2011;3:84ra44. doi:10.1126/scitranslmed.3002230.
18. Dillon M, Yin Y, Zhou J, McCarty L, Ellerman D, Slaga D, Junttila TT, Han G, Sandoval W, Ovacik MA, et al. Efficient production of bispecific IgG of different isotypes and species of origin in single mammalian cells. *MAbs*. 2017;9:213–230. doi:10.1080/19420862.2016.1267089.
19. Schaefer W, Regula JT, Bahner M, Schanzer J, Croasdale R, Durr H, Gassner C, Georges G, Kettenberger H, Imhof-Jung S, et al. Immunoglobulin domain crossover as a generic approach for the production of bispecific IgG antibodies. *Proc Natl Acad Sci U.S.A.* 2011;108:11187–11192. doi:10.1073/pnas.1019002108.
20. Lewis SM, Wu X, Pustilnik A, Sereno A, Huang F, Rick HL, Guntas G, Leaver-Fay A, Smith EM, Ho C, et al. Generation of bispecific IgG antibodies by structure-based design of an orthogonal Fab interface. *Nat Biotechnol*. 2014;32:191–198. doi:10.1038/nbt.2797.
21. Liu Z, Leng EC, Gunasekaran K, Pentony M, Shen M, Howard M, Stoops J, Manchulenko K, Razinkov V, Liu H, et al. A novel antibody engineering strategy for making monovalent bispecific heterodimeric IgG antibodies by electrostatic steering mechanism. *J Biol Chem*. 2015;290:7535–7562. doi:10.1074/jbc.M114.620260.
22. Mazor Y, Oganessian V, Yang C, Hansen A, Wang J, Liu H, Sachsenmeier K, Carlson M, Gadre DV, Borrok MJ, et al. Improving target cell specificity using a novel monovalent bispecific IgG design. *MAbs*. 2015;7:377–389. doi:10.1080/19420862.2015.1007816.
23. Bonisch M, Sellmann C, Maresch D, Halbig C, Becker S, Toleikis L, Hock B, Rüker F. Novel CH1: cL interfaces that enhance correct light chain pairing in heterodimeric bispecific antibodies. *Protein Eng Des Sel*. 2017;30:685–696. doi:10.1093/protein/gzx044.
24. Leabman MK, Meng YG, Kelley RF, DeForge LE, Cowan KJ, Iyer S. Effects of altered FcγR binding on antibody pharmacokinetics in cynomolgus monkeys. *MAbs*. 2013;5:896–903. doi:10.4161/mabs.26436.
25. Sharma VK, Patapoff TW, Kabakoff B, Pai S, Hilario E, Zhang B, Li C, Borisov O, Kelley RF, Chorny I, et al. In silico selection of therapeutic antibodies for development: viscosity, clearance, and chemical stability. *Proc Natl Acad Sci U.S.A.* 2014;111:18601–18606. doi:10.1073/pnas.1421779112.
26. Schlereth B, Quadt C, Dreier T, Kufer P, Lorenczewski G, Prang N, Brandl C, Lippold S, Cobb K, Brasky K, et al. T-cell activation and B-cell depletion in chimpanzees treated with a bispecific anti-CD19/anti-CD3 single-chain antibody construct. *Cancer Immunol Immunother*. 2006;55:503–514. doi:10.1007/s00262-005-0001-1.
27. Sampei Z, Igawa T, Soeda T, Okuyama-Nishida Y, Moriyama C, Wakabayashi T, Tanaka E, Muto A, Kojima T, Kitazawa T, et al. Identification and multidimensional optimization of an asymmetric bispecific IgG antibody mimicking the function of factor VIII cofactor activity. *PLoS ONE*. 2013;8:e57479. doi:10.1371/journal.pone.0057479.
28. Igawa T, Tsunoda H, Tachibana T, Maeda A, Mimoto F, Moriyama C, Nanami M, Sekimori Y, Nabuchi Y, Aso Y, et al. Reduced elimination of IgG antibodies by engineering the variable region. *Protein Eng Des Sel*. 2010;23:385–392. doi:10.1093/protein/gzq009.
29. Bumbaca Yadav D, Sharma VK, Boswell CA, Hotzel I, Tesar D, Shang Y, Ying Y, Fischer SK, Grogan JL, Chiang EY, et al. Evaluating the use of antibody variable region (Fv) charge as a risk assessment tool for predicting typical cynomolgus monkey pharmacokinetics. *J Biol Chem*. 2015;290:29732–29741. doi:10.1074/jbc.M115.692434.
30. Putnam WS, Prabhu S, Zheng Y, Subramanyam M, Wang YM. Pharmacokinetic, pharmacodynamic and immunogenicity comparability assessment strategies for monoclonal antibodies. *Trends Biotechnol*. 2010;28:509–516. doi:10.1016/j.tibtech.2010.07.001.
31. Wang B, Liang M, Yao Z, Vainshtein I, Lee R, Schneider A, Zusmanovich M, Jin F, O'Connor K, Donato-Weinstein B, et al. Pharmacokinetic and pharmacodynamic comparability study of moxetumomab pasudotox, an immunotoxin targeting CD22, in cynomolgus monkeys. *J Pharm Sci*. 2013;102:250–261. doi:10.1002/jps.23343.
32. Nutt SL, Hodgkin PD, Tarlinton DM, Corcoran LM. The generation of antibody-secreting plasma cells. *Nat Rev Immunol*. 2015;15:160–171. doi:10.1038/nri3795.
33. Nagele V, Kratzer A, Zugmaier G, Holland C, Hijazi Y, Ms T, Gökbuget N, Baeuerle PA, Kufer P, Wolf A, et al. Changes in clinical laboratory parameters and pharmacodynamic markers in response to blinatumomab treatment of patients with relapsed/refractory ALL. *Exp Hematol Oncol*. 2017;6:14. doi:10.1186/s40164-017-0074-5.
34. Shatz W, Chung S, Li B, Marshall B, Tejada M, Phung W, Sandoval W, Kelley RF, Scheer JM. Knobs-into-holes antibody production in mammalian cell lines reveals that asymmetric afucosylation is sufficient for full antibody-dependent cellular cytotoxicity. *MAbs*. 2013;5:872–881. doi:10.4161/mabs.26307.
35. Fraker PJ, Speck JC Jr. Protein and cell membrane iodinations with a sparingly soluble chloroamide, 1,3,4,6-tetrachloro-3a,6a-diphenylglycoluril. *Biochem Biophys Res Commun*. 1978;80:849–857.
36. Munson PJ, Rodbard D. Ligand: a versatile computerized approach for characterization of ligand-binding systems. *Anal Biochem*. 1980;107:220–239.
37. Bishop CDVA, Lin Z, Rangell L, Fuh F, Danilenko D, Berry K, Balazs M, Williams M. Characterization of B cell subsets in cynomolgus monkeys. *FASEB J*. 2008;22:847.
38. Carrasco-Triguero M, Davis H, Zhu Y, Coleman D, Nazzal D, Vu P, Kaur S. Application of a plug-and-play immunogenicity assay in cynomolgus monkey serum for ADCs at early stages of drug development. *J Immunol Res*. 2016;2016:2618575. doi:10.1155/2016/2618575.